04

Radial distribution of emitting centers in Ar laser plasma

© V.E. Guseva, A.N. Nechay, A.A. Perekalov, N.I. Chkhalo

Institute of Physics of Microstructures, Russian Academy of Sciences,
607680 Nizhny Novgorod, Russia
e-mail: valeriegus@ipmras.ru

Received May 29, 2025
Revised May 29, 2025
Accepted May 29, 2025

In this work the images of an argon spark in the extreme ultraviolet (EUV) range obtained using an EUV microscope with an operating wavelength of 11.25 nm were studied. The gas target formed by the gas jet flowing into a vacuum chamber from a conical supersonic nozzle at a gas pressure of 3−10 bar at the nozzle inlet. An Nd:YAG- laser ($\lambda = 1064$ nm, $\tau_{imp} = 4.2$ ns) with a pulse energy of 0.4−0.8 J was used for excitation. Image processing was carried out using the inverse Abel transform method due to the presence of axial symmetry of the spark relative to the laser beam axis. As a result of the work, radial distributions of radiating centers in an argon spark at a wavelength of 11.25 nm were obtained for various excitation parameters.

Keywords: laser spark, EUV radiation, gas-jet targets.

DOI: 10.61011/TP.2025.09.61836.122-25

Introduction

Sources of soft X-ray (SX) and extreme ultraviolet (EUV) radiation are now increasingly being used for various applications such as X-ray microscopy, reflectometry, or lithography. The greatest attention is paid to laser-plasma sources (LPS) among the sources of EUV radiation. Various gases [1,2] and liquids [3], as well as solid-state targets [4–6], can be used as targets for producing laser plasma in LPS.

A xenon-based gas jet target is one of the promising radiation sources for EUV lithography at a wavelength of 11.25 nm [7]. Xenon laser plasma emits in a wide high-intensity emission band in the vicinity of 11 nm [8,9], and modern multilayer X-ray mirrors (MXM) based on the multilayer Mo/Be system make it possible to effectively use the radiation of this band in various X-ray optical devices, such as the X-ray lithograph [7,10].

In addition to high radiation intensity, a requirement for the source size is also imposed on EUV radiation sources for lithographic applications. The characteristic size of the source should be on the order of 500 m, which corresponds to the size of the spark area from where the radiation is captured by the collector. Thus, for successful integration of the radiation source and the X-ray optical system, it is necessary to know the size of the spark and the distribution of radiation centers in it.

In addition to practical applications, the study of spark structure in gas-jet LPS is also of interest from a fundamental point of view. Despite the fact that laser plasma has been studied for quite a long time, the processes occurring in a laser spark are still insufficiently studied. Most of the papers related to the study of LPS are aimed at studying the emission spectra [11,12] and increasing the conversion coefficient of laser radiation to short-wavelength [9]. The study of the distribution of radiating centers in laser sparks has received significantly less attention in the literature. Of particular interest are studies of images of laser sparks and the distribution of radiating centers in laser sparks detected in the EUV spectral range.

In this work, the radial distribution of the EUV radiation centers of a laser plasma formed when an argon-based gas jet target is excited by pulsed Nd:YAG-laser radiation was studied. Argon is a convenient model object for studying the distribution of centers emitting in the EUV spectral range in a laser spark. The convenience of argon consists in the low absorption of radiation at a wavelength of 11.25 nm in the argon plasma itself, which makes it quite easy to process the resulting images of a laser spark.

The images of the laser spark were obtained using a quintuple-magnification EUV microscope based on a Schwarzschild lens. Ar VII ions mainly emit at the operating wavelength of the microscope of 11.25 nm in an argon laser plasma in case of excitation by Nd:YAG-laser with a pulse duration of ~ 4.2 ns and an energy of ~ 0.8 J. The inverse Abel transform method was used to determine the radial distribution of the radiating centers in the spark region [13,14]. The possibility of using this method is attributable to the axial symmetry of the laser spark relative to the axis of the laser beam.

1. Experimental technique

The experiment consisted in obtaining images of a laser spark at a wavelength of 11.25 nm, formed when an argon gas jet target is excited by pulsed neodymium laser radiation. The scheme of the experimental setup is shown in Fig. 1. The axes x, y and z are located perpendicular to each other.

The experiment was as follows: the impulse gas-jet target was formed with the gas leaving the conic ultrasound nozzle *1* into the vacuum chamber *2*. The optical path of the laser radiation to the target consists of a dividing plate *5*, which deflects a small part of the radiation into the IMO-2 6 power detector, and a prism *7*, which directs the radiation into the entrance window *8* of the vacuum chamber *2*. The radiation of a pulsed Nd:YAG-laser *4* was focused on a gas-jet target with a lens *3* with a focal length of 45 mm. In a focusing point, the laser-induced breakdown results in generation of highly-ionized plasma *9*. The experimental setup is described in more detail in Ref. [15].

The laser spark images were obtained by directing plasma radiation into an inlet of the double-mirror X-ray microscope *10* with fivefold magnification (Fig. 1), which was assembled in the Schwarzschild scheme. Laser plasma radiation in the EUV spectral range was detected using two free-hanging filters based on Zr/SiZr *11* and *12* located at the inlet and exit of the microscope. The multilayer X-ray mirrors it 13 and it 14 used in the microscope, located on the lens surface, are based on Mo/Be structures reflecting radiation at a wavelength of 11.25 nm with a peak reflection coefficient of $\sim 67\,\%$. The spectral dependences of the reflection coefficients of the mirrors *13* and *14* are shown in Fig. 2. The microscope-built image is projected to a receiving matrix detector *15* GSENSE 2020 BSI, which uses the CMOS technology. More details on the design and the characteristics of the microscope are given in Ref. [16].

Nd:YAG-laser with a wavelength of $\lambda = 1064$ nm, pulse duration and energy of $\tau = 4.2$ ns and $E = 0.4–0.8$ J, respectively, was used during the experiment. The pulse repetition frequency was 2 Hz. The optical system focused the laser radiation into a spot with a diameter of $\sim 60\,\mu$m. The power density of the laser radiation in the focus area was $\sim 6 \cdot 10^{12}$ W/cm^2. A supersonic conical nozzle with a critical cross section of $d_{cr} = 500\,\mu$m, length of $l = 5$ mm and a half-angle of the opening $\alpha/2 = 4.5°$ was used to supply gas. The gas pressure at the nozzle inlet ranged

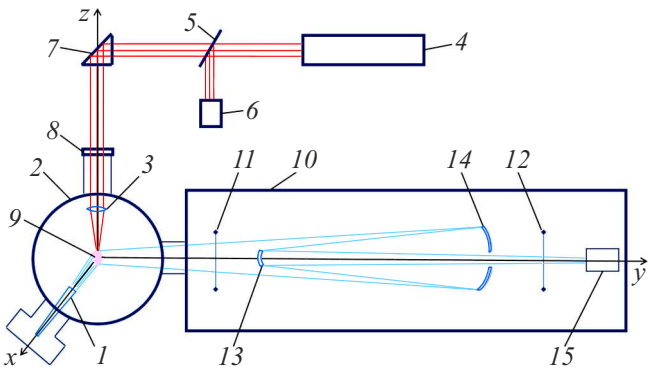

Figure 1. Experimental setup diagram: *1* — supersonic conical nozzle, *2* — vacuum chamber, *3* — focusing lens, *4* — Nd:YAG-laser, *5* — dividing plate, *6* — IMO-2 power detector, *7* — prism, *8* — introductory window, *9* — laser spark, *10* — X-ray microscope, *11, 12* — Zr/SiZr-film filters, *13* — convex MXM, *14* — concave MXM, *15* — matrix CMOS detector.

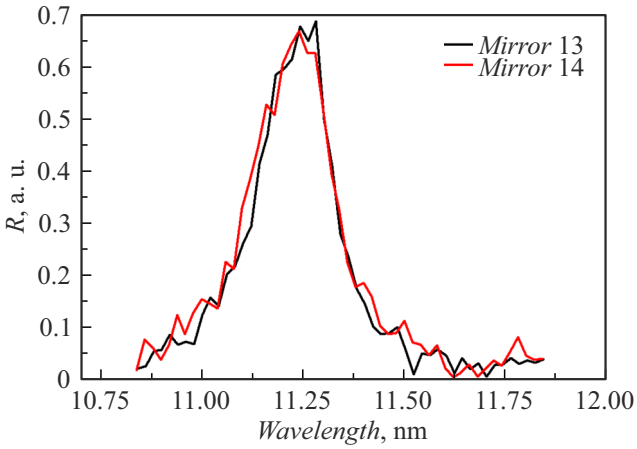

Figure 2. Spectral dependences of reflection coefficients of mirrors M1 and M2.

from 3 to 10 bar, and the temperature was 300 K. The pressure in the vacuum chamber was maintained at the level of 10^{-2} Pa. The laser spark was located at a distance of 0.5 mm from the nozzle tip.

A signal from several laser pulses was accumulated to obtain an image of argon sparks emitting weakly at a wavelength of 11.25 nm.

2. Experiment and results obtained

The images of argon laser sparks at a wavelength of 11.25 nm obtained using an EUV microscope are shown in Fig. 3. The laser beam in the images is directed from above. The nozzle edge and the laser axis are shown schematically in the photographs. Images of sparks are shown at the following parameters of the laser pulse and gas pressure: $E_{imp} = 0.4$ J, $p_{gas} = 8$ bar; $E_{imp} = 0.8$ J, $p_{gas} = 8$ bar; $E_{imp} = 0.8$ J, $p_{gas} = 4$ bar.

It can be seen that all the sparks have a shape elongated along the laser beam. The length of the argon spark is $\sim 800\,\mu$m for different excitation parameters. The diameter and intensity of the spark emission are not the same for different parameters of the gas jet and the laser pulse. A laser spark of the smallest diameter $\sim 180\,\mu$m is observed at a laser pulse energy of 0.4 J and an argon pressure of 8 bar. A laser spark with the largest diameter $\sim 250\,\mu$m is observed at a laser pulse energy of 0.8 J and an argon pressure of 4 bar.

In total, during a series of experiments, images of an argon laser spark were obtained at an energy of exciting laser radiation in the range from 0.4 to 0.8 J at a gas pressure at the nozzle inlet of 8 bar and at a gas pressure at the nozzle inlet in the range from 3 to 10 bar at a laser pulse energy 0.8 J.

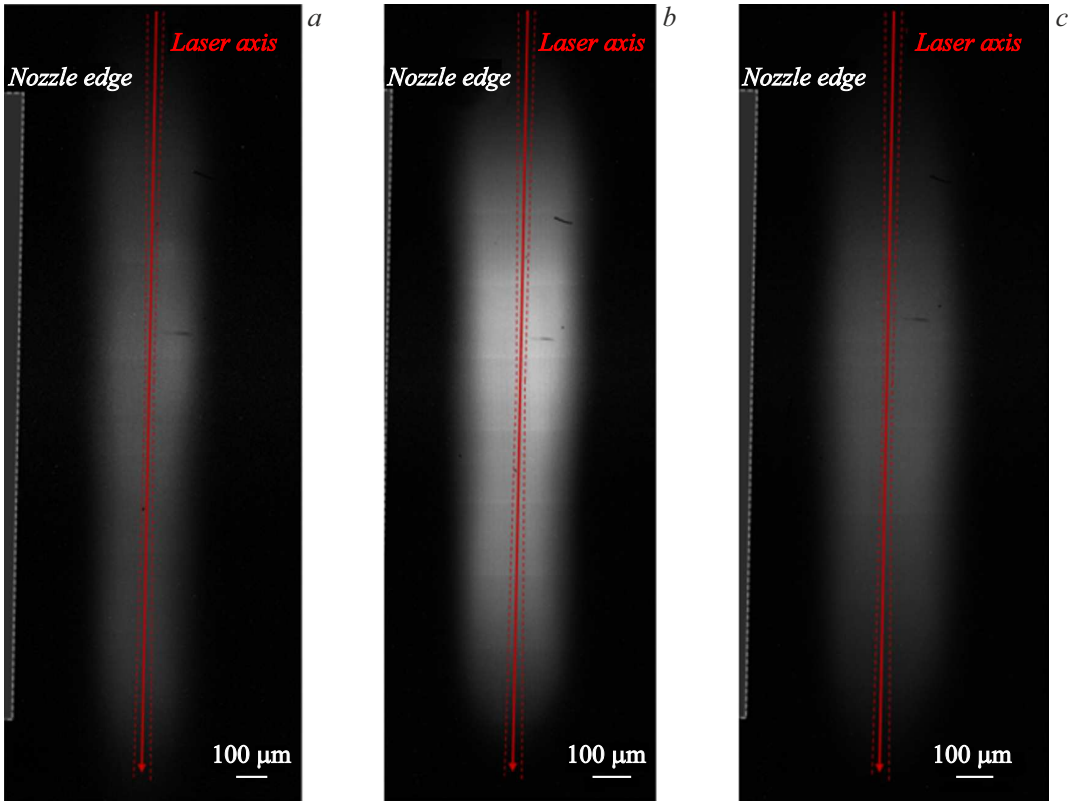

Figure 3. Images of argon laser sparks obtained using an EUV microscope at a wavelength of 11.25 nm: *a* — $E_{imp} = 0.4$ J, $p_{gas} = 8$ bar; *b* — $E_{imp} = 0.8$ J, $p_{gas} = 8$ bar; *c* — $E_{imp} = 0.8$ J, $p_{gas} = 4$ bar.

3. Experimental data processing methodology

For a laser spark, there is an axial symmetry relative to the axis of the laser beam. In such cases, the spatial distribution of the radiation centers in the spark is a function of only two coordinates in the cylindrical system $I = I(r, z)$. Let $P(x, z)$ be a two-dimensional projection of $I(r, z)$ onto the detector plane (x, z), where the axis x is perpendicular to the axis z. These two functions are linked by a direct Abel integral:

$$P(x, z) = 2 \int_{|x|}^{\infty} \frac{rI(r, z)}{\sqrt{r^2 - x^2}} dr.$$

The images of the laser spark obtained in the experiment are a flat projection of the spark radiation $P(x, z)$ on a two-dimensional grid of 2048×2048 pixels, where 1 pixel = 1.3 m. Then the radial distribution of the radiating centers $I(r, z)$ can be obtained by calculating the inverse Abel transform:

$$I(r, z) = -\frac{1}{\pi} \int_{r}^{\infty} \frac{[dP(x, z)dx]}{\sqrt{x^2 - r^2}} dx.$$

This method works in conditions where self-absorption of EUV radiation in plasma can be neglected. The experimentally obtained data require preliminary smoothing to the extent that noise of various nature is suppressed, but the fundamental physical picture is preserved.

The Abel transform was performed using the ready-made Idea program and code written using the PyAbel library of functions in Python. Despite the fact that Idea is a ready-made, proven solution, the main disadvantage of the program is the ability to work only with two-dimensional data arrays. Thus, using the Idea program, it is possible to study only sections of a spark in a cross-section, represented as a dependence of intensity on a coordinate along the axis x with a fixed coordinate along the axis z. Unlike the Idea program, the PyAbel library of functions in Python can work with three-dimensional data arrays, i.e. with the entire image as a whole, defined as a matrix of intensity values with coordinates along the axes x and z.

The following image processing procedure was performed to use the inverse Abel transform on experimentally obtained images of an argon laser spark. The position of the axis of symmetry of the spark was determined and the image of the spark was rotated so that the axis of symmetry was vertical. Next, the image, represented by a matrix of intensity values in each pixel, was row-by-row averaged over the right and left halves of the image relative to the axis of symmetry. This is necessary to reduce the error of the experimental data and achieve their complete symmetry. Further, a one-dimensional Gaussian filter was applied to the dependence of the radiation intensity for each spark

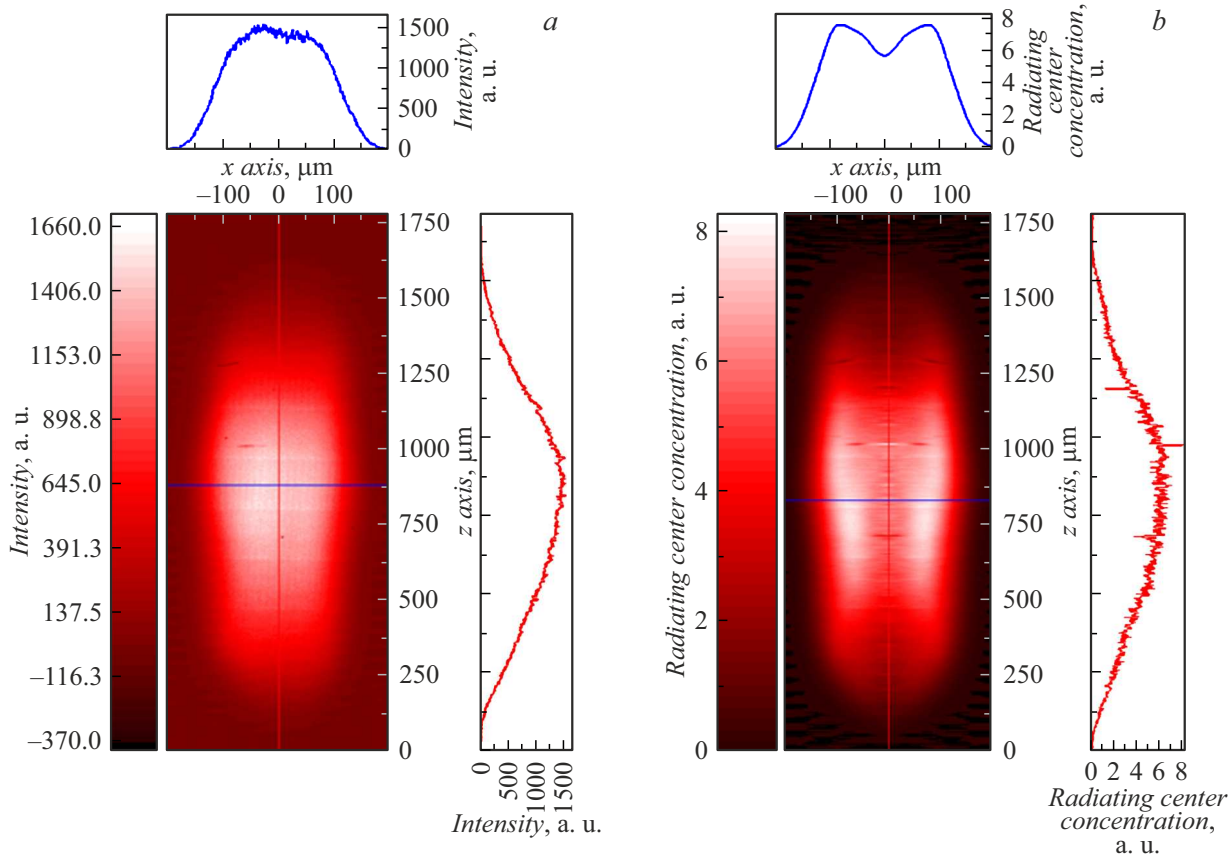

Figure 4. Image of a spark (*a*) and radial distribution of radiating centers (*b*) in argon sparks at a gas pressure of 5 bar and a laser pulse energy of 0.8 J.

section in order to smooth out the high-frequency noise of the radiation receiver. The standard deviation for the Gaussian kernel was 6–7, depending on the intensity of the image. Then the inverse Abel transform is applied to each spark cross-section (to each radiation dependence in a given section). The resulting transformation matrix for half of the image is mirrored and combined with the first half. This results in a distribution of radiating centers for the complete image of the laser spark. For received images, the coordinate values are recalculated from pixels to micrometers.

In this paper, we used the Abel transform algorithm „Direct“ from the PyAbel library of functions in Python. This method makes no assumptions about the source data, except for cylindrical symmetry, and is a direct numerical integration of the inverse Abel transform function. This method is described in more detail in Ref. [17]. The result of the „Direct“ conversion was compared with the results obtained by other methods from the PyAbel library of functions in Python. When using other methods, the result of the inverse Abel transform coincided with the chosen „Direct“conversion method. Also, the conversion result obtained for one spark section in the Idea program was qualitatively the same as the result of the conversion of the same section using the „Direct“ method. We confirmed the reversibility of the transformation in the case under study by performing a direct Abel transform for the inversely transformed image and comparing the result with the original data.

In practice, when performing the reverse Abel transform to restore the concentration of emitting centers in a laser spark in the EUV range and, in particular, at a wavelength of 11.25 nm, it is necessary to take into account the self-absorption of EUV radiation in plasma, since self-absorption can significantly affect the results obtained. There are no intense emission lines in the argon spectrum near the studied wavelength of 11.2 nm, so it can be stated with great confidence that self-absorption in plasma at this wavelength is low, and the observed pattern is determined by the redistribution of radiating centers.

4. Discussion of the results

As a result of the experiment, images of laser sparks at a wavelength of 11.25 nm were obtained, formed when an argon target was excited, and they were processed using the reverse Abel transform. Fig. 4 shows an image of an argon laser spark at a wavelength of 11.25 nm (Fig. 4, *a*) and the radial distribution of radiating centers in an argon spark (Fig. 4, *b*) obtained using the Abel transform, at a gas pressure at the nozzle inlet of 5 bar and a laser pulse energy

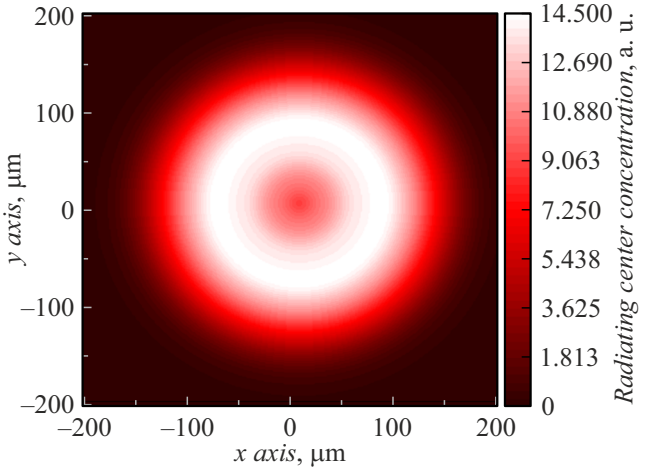

Figure 5. Distribution of radiating centers in the argon spark section, reconstructed from the results of the inverse Abel transform.

of 0.8 J. The upper and lateral graphs of each figure show the transverse and longitudinal profiles of the spark section, respectively. The sections correspond to the lines shown in the image. The coordinates are given in micrometers, the radiation intensity (Fig. 4, *a*) and the concentration of radiating centers (Fig. 4, *b*) are given in relative units. The laser radiation in the images is directed from top to bottom.

The spark image is elongated, with a width-to-length ratio of about 1 to 3. The cross-sectional distribution of the radiation intensity in the detector plane has the shape of a plateau. After the Abel transform, it becomes clear that the intensity distribution in the shape of a single wide peak is formed due to two peaks in the cross-section of the spatial distribution of the concentration of radiating centers. The shape of the spark cross-section, reconstructed from the distribution of the radiating centers, is shown in Fig. 5. The shape of the distribution of radiating centers at a wavelength of 11.25 nm in an argon laser spark in space is close to the shape of a tube. The cross section of the distribution of radiating radiation centers is close to the shape of the ring.

The diameter of the central region with a reduced concentration of radiating centers is $\sim 60\,\mu$m in width at half height, which is close to the diameter of the laser beam at the point of focus. The decrease in the concentration of radiating centers in this region is $\sim 20\,\%$. Most of the radiation centers at a wavelength of 11.25 nm in argon sparks are shifted closer to the edge of the spark. Physically, this pattern corresponds to a redistribution of the radiating centers and, consequently, a shift in gas concentration from the axial part of the spark to its edges, probably due to the formation of a shock wave.

The image of a laser spark that we observe is a time-integral picture, since the laser spark significantly changes its shape during registration. Initially, we observe a radiating cylinder, then an expanding cavity forms along the axis of the expanding radiating cylinder, which probably corresponds to the formation of a cylindrical shock wave. The superposition of all the described images forms the observed image and the distribution of radiating centers. Thus, the presence of features corresponding to the propagation of the shock wave, even on the time-integral distribution of the radiating centers, indicates the possible influence of the shock wave on the distribution of the radiating centers.

Fig. 6 shows the time-averaged radial distributions of the radiating centers at argon inlet pressures in the range of 3–10 bar. The laser beam falls from above. The energy of the laser pulse is 0.8 J. The color ranges correspond to the areas 0 %–5 %, 5 %–50 %, 50 %–85 %, 85 %–95 % and higher than 95 % from the maximum concentration of radiating centers. The coordinates are given in micrometers, the concentrations of the radiation centers are in relative units.

It can be seen that all the sparks are elongated. As the pressure increases from 3 to 10 bar, the width-to-length ratio decreases from 1 to 2.5 to 1 to 4 by increasing the spark length. The radial distribution of radiating centers with a reduced concentration in the center is preserved for all argon pressures. The maximum concentration of radiating centers shifts upward towards the laser beam with increasing pressure, while the spark volume increases with the maximum concentration of radiating centers. Thus, the extension of the tube from radiating centers towards the laser beam is observed.

Fig. 7 shows the transverse profiles of the radial distribution of the radiating spark centers at argon inlet pressures in the range of 3–10 bar. The energy of the laser pulse is 0.8 J. The sections were drawn through the central spark region with the maximum concentration of radiation centers for each pressure. The concentrations of the radiating centers are given in relative units, the coordinate of the transverse axis is given in micrometers.

It can be seen from Fig. 7, *a* that the number of radiation centers increases significantly with increasing pressure. When the pressure is doubled (from 5 to 10 bar), their concentration increases by 2.2 times. At the same time, it can be seen from the normalized graphs in Fig. 7, *b* that the width of the spark at half height does not change significantly with increasing pressure from 3 to 10 bar and is $\sim 250\,\mu$m. The distance between the peaks changes little in the first approximation (a narrowing of the order of 25 %). The diameter of the central region with a reduced concentration of radiating centers varies from 90 to 60 μm in width at half height with an increase in pressure from 3 to 10 bar.

The observed pattern can be explained as follows. The elongated shape of the calf is caused by the movement of the „laser detonation wave“ [18,19]. The gas heated to high temperatures in the breakdown region expands rapidly, forming a shock wave [9,13], moving both along the axis of the laser beam and perpendicular to it. The shift of the concentration of radiating centers from the center of the spark corresponds to the propagation of the shock wave in the direction perpendicular to the axis of the laser beam.

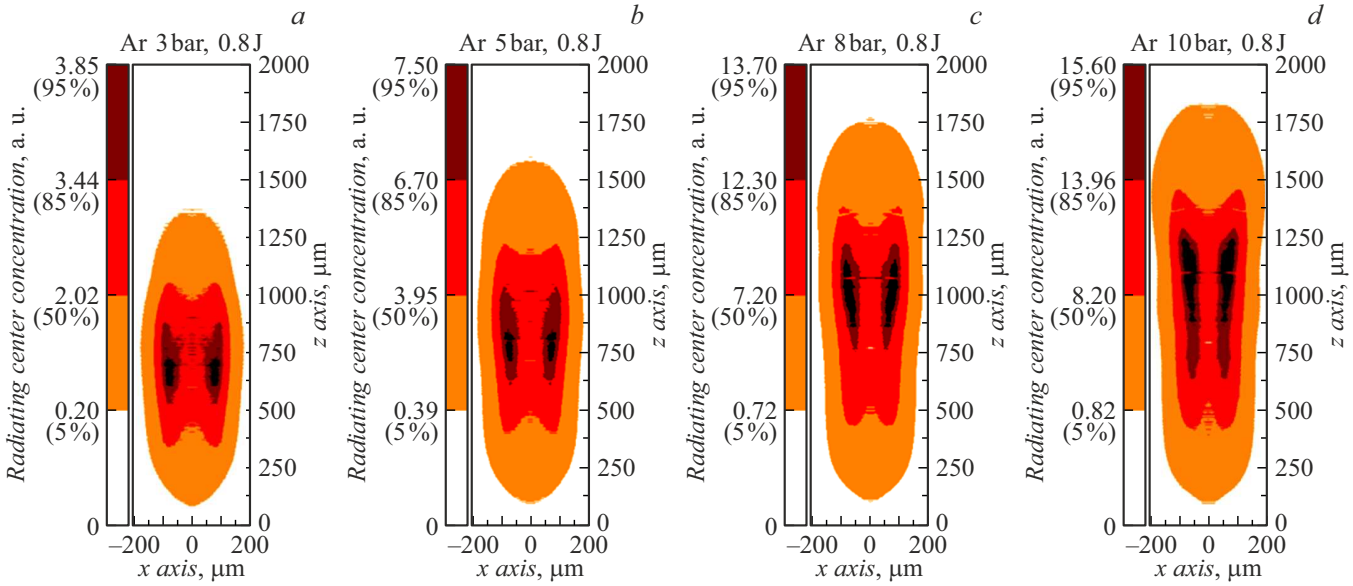

Figure 6. Radial distributions of radiating centers at argon pressures at inlet to nozzle 3 (*a*), 5 (*b*), 8 (*c*) and 10 (*d*) bar.

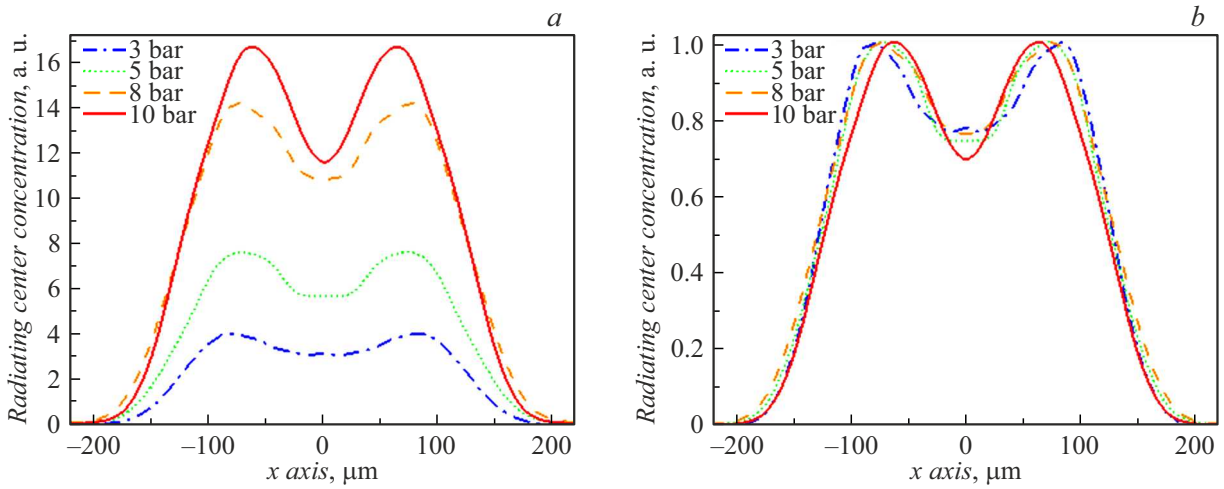

Figure 7. Transverse profiles of the radial distribution of radiating spark centers at different pressures without normalization (*a*) and normalized by one (*b*).

The absorption of laser radiation by the target is proportional to the density of the target. As the gas density increases, the intensity of the spark radiation generally increases due to an increase in the number of emitting particles. At the same time, at different target densities, the amount of energy absorbed in the gas per the number of absorbing particles is approximately preserved, and thus the spark width and the distance between the peaks also change little. And the concentration of radiation centers increases due to the absorption of a greater proportion of the energy of the laser pulse.

Fig. 8 shows the radial distributions of argon emitting centers at an exciting laser pulse energy of 0.4–0.6 J and a gas pressure of 8 bar. The laser beam falls from above. The color ranges correspond to the areas 0%–5%, 5%–50%, 50%–85%, 85%–95% and above 95% of the maximum concentration of radiating centers. The coordinates are given in micrometers, the concentrations of the radiating centers are given in relative units.

It can be seen that all the sparks are elongated. As the energy increases, the width-to-length ratio (FWHM) changes from 1/5 at $E = 0.4$ and 0.6 J to 1/3.5 at $E = 0.8$ J. The radial distribution of the radiating centers in the shape of a tube is preserved for all laser pulse energies. The maximum concentration of radiating centers remains in a position slightly above the geometric center of the spark, while the volume of the spark with the maximum concentration of radiating centers is stretched towards the laser beam with increasing energy.

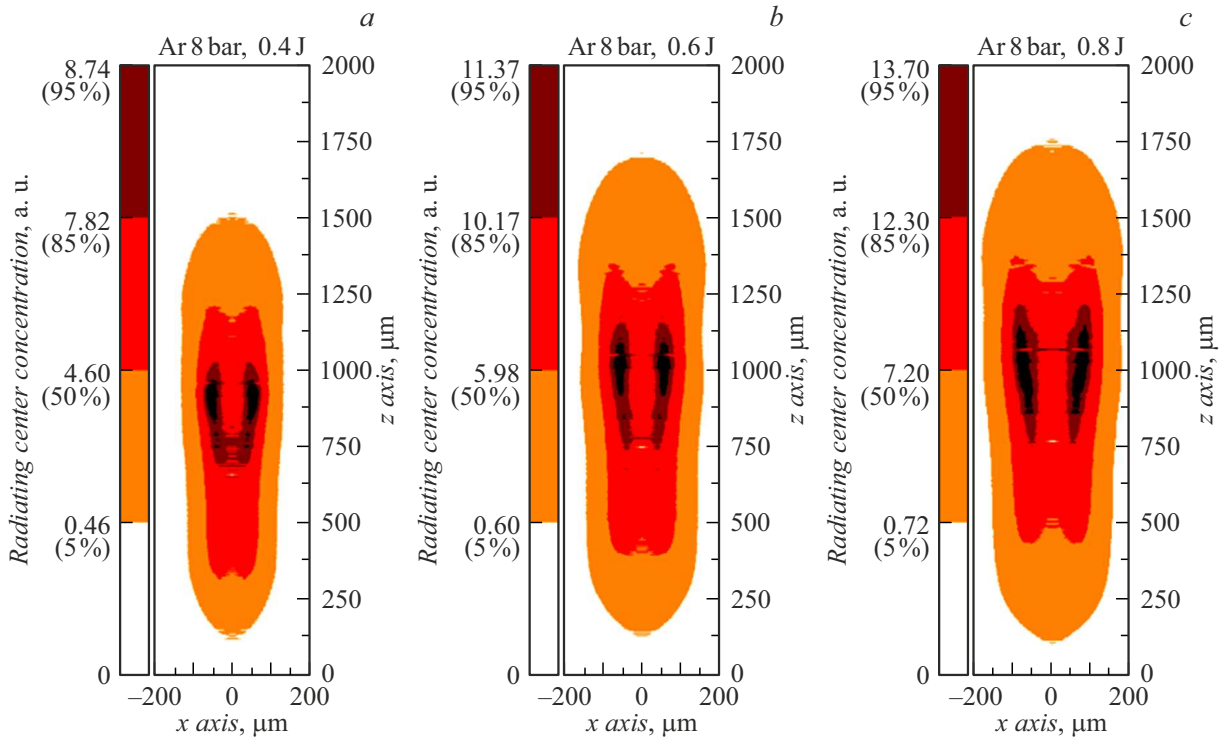

Figure 8. Radial distributions of radiating centers in argon spark at laser pulse energies of 0.4 (*a*), 0.6 (*b*) and 0.8 J (*c*).

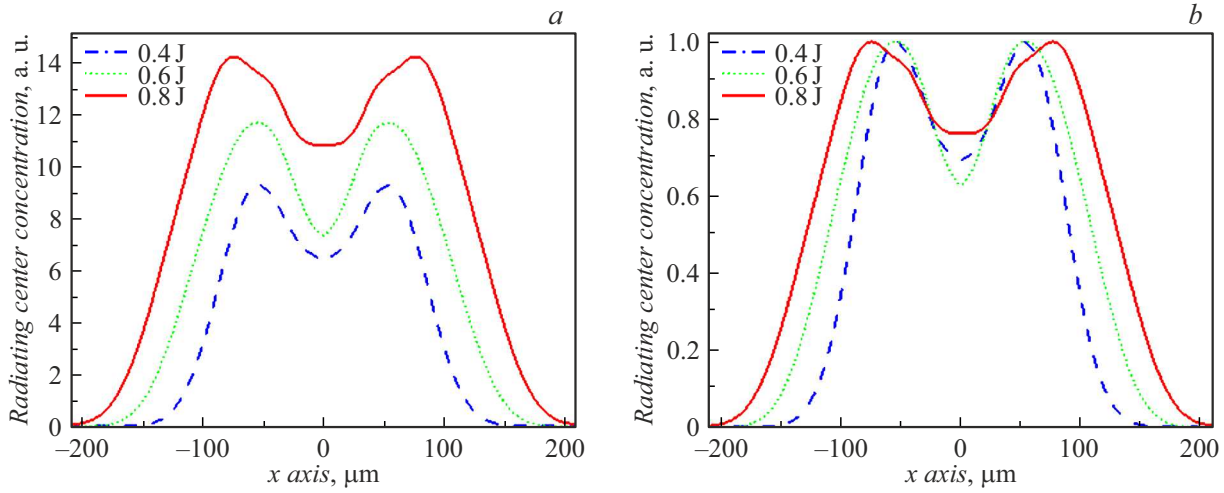

Figure 9. Transverse profiles of the radial distribution of the radiating spark centers at different laser energies without normalization (*a*) and normalized by one (*b*).

Fig. 9 shows the transverse profiles of the radial distribution of the radiating centers of an argon spark when excited by laser pulses with energies from 0.4 to 0.8 J. The gas pressure at the nozzle inlet is 8 bar. The cross sections were drawn through the central region of the spark with the maximum concentration of radiation centers for each energy value. The concentration of radiating centers is given in relative units, the coordinate of the transverse axis is — in micrometers.

It can be seen from Fig. 8, *a* that as the excitation energy increases, both the concentration of radiation centers and the spark width increase. When the energy is doubled (from 0.4 to 0.8 J), the concentration increases by 1.5 times. The spark width at energies of 0.4, 0.6, and 0.8 J is 180, 190, and 250 μm, respectively. The distance between the peaks also changes little (a broadening of the order of 25%). The diameter of the central region with a reduced concentration of radiating centers does not change with increasing laser pulse energy and is $\sim 60\,\mu$m.

As the energy of the laser pulse increases, the diameter of the spark and the mass of the entrained gas increase. An increase in the number of emitting particles and a

corresponding increase in their concentration is observed. At the same time, the ratio of energy to the number of absorbing particles E/n is not preserved. The amount of energy per the number of atoms in the spark volume increases, which probably forms a detonation wave of greater intensity and temperature, which corresponds to an increase in the spark diameter.

Conclusions

The inverse Abel transform was used to process images of an argon laser spark at a wavelength of 11.25 nm. Thus, the radial distribution of radiating centers in an argon spark was obtained under various excitation conditions. The following conclusions can be drawn based on the results of the work carried out:

1. An argon laser spark has a shape elongated along the axis of the laser beam with the studied excitation parameters — pressure from 3 to 10 bar, and the laser pulse energy from 0.4 to 0.8 J. The distribution of radiating centers in the argon spark has the shape of a tube, which is probably due to the movement of the shock wave from the breakdown region. The shape of the tube for the radiation centers in the argon spark is preserved for all the studied excitation parameters.

2. As the jet density increases due to changes in gas pressure, the absorption of laser radiation increases in proportion to the number of absorbing particles. The diameter of the spark remains constant, and the concentration of radiating centers increases due to an increase in their number.

3. As the energy of the laser pulse increases, the energy input in the absorption zone of the laser radiation increases, which leads to an increase in the diameter of the spark and an increase in the volume of gas involved in the process.

Funding

Theoretical part of the work was carried out within the framework of the state assignment FFUF-2024-0022. The experiment was conducted with the support of the Russian Science Foundation grant 21-72-30029-P.

Conflict of interest

The authors declare that they have no conflict of interest.

References

[1] V.G. Kapralov, R. Korde, V.E. Levashov, A.S. Pirozhkov, E.N. Ragozin. Kvantovaya elektronika, **32** (2), 149 (2002) (in Russian).
[2] A.S. Boldarev, V.A. Gasilov, V.E. Levashov, K.N. Mednikov, A.S. Pirozhkov, M.S. Pirozhkova, E.N. Ragozin. Kvantovaya elektronika, **34** (7), 679 (2004) (in Russian).
[3] D.B. Abramenko, P.S. Antsiferov, D.I. Astakhov, A.Yu. Vinokhodov, I.Yu. Vichev, R.R. Gayazov, A.S. Grushin, L.A. Dorokhin, V.V. Ivanov, D.A. Kim, K.N. Koshelev, P.V. Krainov, M.S. Krivokorytov, V.M. Krivtsun, B.V. Lakatosh, A.A. Lash, V.V. Medvedev, A.N. Ryabtsev, Yu.V. Sidelnikov, E.P. Snegirev, A.D. Solomyannaya, M.V. Spiridonov, I.P. Tsygvintsev, O.F. Yakushev, A.A. Yakushkin. UFN, **189** (3), 323 (2019) (in Russian).
[4] E.A. Vishnyakov, K.N. Mednikov, A.A. Pertsov, E.N. Ragozin, A.A. Reva, A.S. Ulyanov, S.V. Shestov. Kvantovaya elektronika, **39** (5), 474 (2009) (in Russian).
[5] I.L. Beigman, E.A. Vishnyakov, M.S. Luginin, E.N. Ragozin, I.Yu. Tolstikhina. Kvantovaya elektronika, **40** (6), 545 (2010) (in Russian).
[6] A.O. Kolesnikov, E.A. Vishnyakov, E.N. Ragozin, A.N. Shatokhin. Kvantovaya elektronika, **50** (10), 967 (2020) (in Russian).
[7] N.I. Chkhalo, K.V. Durov, A.N. Nechay, A.A. Perekalov, V.N. Polkovnikov, N.N. Salashchenko. J.Surface Investigation: X-ray, Synchrotron and Neutron Techniques, **17** (1), 226 (2023).
[8] V.E. Guseva, A.N. Nechay, A.A. Perekalov, N.N. Salashchenko, N.I. Chkhalo. Appl. Phys. B, **129**, 155 (2023).
[9] S.G. Kalmykov, P.S. Butorin, M.E. Sasin. J. Appl. Phys., **126** (10), 103301 (2019).
[10] M.V. Svechnikov, N.I. Chkhalo, S.A. Gusev, A.N. Nechay, D.E. Pariev, A.E. Pestov, V.N. Polkovnikov, D.A. Tatarskiy, N.N. Salashchenko, F. Schäfers, M.G. Sertsu, A. Sokolov, Y.A. Vainer, M.V. Zorina. Opt. Express, **26** (26), 33718 (2018).
[11] H. Fiedorowicz, A. Bartnik, R. Jarocki, J. Kostecki, J. Krzywiński, J. Mikołajczyk, R. Rakowski, A. Szczurek, M. Szczurek. J. Alloys Compounds, **401** (1-2), 99 (2005).
[12] A.V. Vodop'yanov, S.A. Garakhin, I.G. Zabrodin, S.Yu. Zuev, A.Ya. Lopatin, A.N. Nechay, A.E. Pestov, A.A. Perekalov, R.S. Pleshkov, V.N. Polkovnikov, N.N. Salashchenko, R.M. Smertin, B.A. Ulasevich, N.I. Chkhalo. Quant. Electron., **51** (8), 700 (2021).
[13] N.Y. Bakaev, N.G. Basov, V.P. Varava, A.I. Veretennikov, A.A. Galicii, E.I. Ershov, M.P. Kalashnikov, Yu.A. Mikhailov, A.V. Rode, G.V. Sklizkov, R.P. Tarasov, S.I. Fedotov. Kvantovaya elektronika, **9** (9), 1750 (1982) (in Russian).
[14] K. Bockasten. JOSA, **51** (9), 943 (1961).
[15] A.N. Nechai, A.A. Perekalov, N.I. Chkhalo, N.N. Salashchenko, I.G. Zabrodin, I.A. Kaskov, A.E. Pestov. Poverkhnost. Rentgenovskie, sinhrotronnye i neitronnye issledovaniya **9**, 83 (2019) (in Russian).
[16] A.A. Perekalov, V.E. Guseva, I.V. Malyshev, A.N. Nechay, A.E. Pestov, D.G. Reunov, R.M. Smertin, M.N. Toropov, N.N. Tsybin, N.I. Chkhalo. Rev. Scientific Instruments. (2023).
[17] V. Dribinski, A. Ossadtchi, V.A. Mandelshtam, H. Reisler. Rev. Scientific Instruments, **73** (7), 2634 (2002).
[18] B. Zel'dovich, Yu.P. Raizer. *Fizika udarnykh voln i vysokotemperaturnykh gidrodinamicheskikh yavlenii* (Nauka, M., 1974) (in Russian).
[19] Yu.P. Raizer. *Lazernaya iskra i rasprostraneniye razryadov* (Nauka, M., 1974) (in Russian).

Translated by A.Akhtyamov